Analysis of crack parameters under mixed mode loading by modified exponential matrix method

J.M. Nianga, F. Mejni, T. Kanit, A. Imad, J. Li

Version of Record: https://www.sciencedirect.com/science/article/pii/S0167844218306293
Manuscript_a701a73cca6b30fa78ecea0ab0a8110c

Analysis of Crack Parameters under Mixed Mode Loading by Modified Exponential Matrix Method

J. M. Nianga [1], F. Mejni [1], T. Kanit [2, 4], A. Imad [2] and J. Li [3]

1. Hautes Etudes d'Ingénieur, Lille, France
2. Unité de mécanique de Lille, EA7512, Université de Lille, Villeneuve-d'Asq, France
3. Laboratoire des Sciences des Procédés et des Matériaux, UPR3407,Villetaneuse, France
4. Corresponding author: tkanit@univ-lille.fr

Abstract

This paper deals with a new analytical method, the exponential matrix method EMM, for calculating the T-stress and the stress intensity factors SIFs under mixed mode loading. The linear, elastic, two-dimensional and stationary equations of the crack problem are transformed into a Hamiltonian system. This is solved by the proposed method involving eigensolutions which satisfy the adjoint symplectic orthogonality by means of performing an angular stress variation with respect to the radial stress. A good description of the expected solution of the studied problem is then obtained as a linear combination of these eigensolutions. To illustrate the validity of the present method, some numerical examples are used and the results obtained are compared with those of literature.

Keywords

Exponential Matrix Method MEM; Stress Intensity Factor SIF; T-Stress; Mixed Mode; Symplectic method

1. Introduction

In fracture mechanics, the description of the stress field at the vicinity of the crack tip is generally described by the stress intensity factors SIFs and possibly for brittle materials, by a non-singular stress acting parallel to the crack face, the so-called T-stress Larsson and Carlsson (1973); Rice (1974). One of the interests in the calculation of the T-stress is the evaluation of its effect on the stability of the crack path direction, as examined by Cotterell (1966); Melin (2002); Fett and Munz (2003).
In some cases, the description may involve high-order terms of Williams' asymptotic expansion Williams (1960). This allows taking the superposition of the main failure modes into account, in particular the modes *I* and *II*. On the other hand, the combination of the T-stress and SIFs provides a better understanding of the behavior of materials at the crack tip Gupta *et al.* (2015). A little less than twenty years ago, Dyskin (1997) established the influence of the higher-order terms of Williams' asymptotic expansion on the size effect, for quasi-brittle materials.
In the following, the studied material is assumed to be subjected to mixed mode $I+II$ conditions. These express a superimposition of the transverse tensile loading mode I and the in-plane shear loading mode II, characterized by the SIFs K_I and K_{II} respectively. The mixed mode fracture is the mode that characterizes most practical fracture problems. Indeed, most structures are not uniquely subjected to a single loading mode. They are most often subjected to a combination of at least two of the three main modes I, II and III due to a particular orientation of crack surfaces, multiaxial loads or mixed mode loads, respectively. Numerous studies have been devoted to mixed mode loading analysis. The significant

influence of the T-stress on brittle fracture in linear elasticity, under mixed mode conditions, was studied by Smith *et al.* (2001) and Karihaloo (1999).
Recent studies contribute comprehensively to a better understanding of mixed mode fracture Demir *et al.* (2017); Pirmohammad and Hojjati Mengharpey (2018). Initial investigations on this subject date back almost fifty years Erdogan and Sih (1963). Holston (1976) presented a special finite element for plane analysis of elastic structures with cracks through the thickness, to include the in-plane shearing K_{II} mode of deformation, obtaining results applicable to K_{I} and $K_I + K_{II}$ modes of deformation. Several years later, Ramaswamy *et al.* (1993) used a modified flexural specimen and an optical shearing interferometry to analyze mixed mode crack tip deformations. They obtained the measurement of some crack tip parameters such as stress-intensity factors, on the basis of Williams' mixed mode asymptotic expansion. Interested in quasi-static crack under mixed mode loading conditions, Chalivendra (2009) studied an inhomogeneous orthotropic medium, using an asymptotic analysis coupled with the Westergaard stress function. Stepanova and Yakovleva (2016) used the perturbation method to obtain asymptotic solutions to nonlinear eigenvalue problems, when studying stress-strain fields in the vicinity of a crack tip under mixed mode loading. Machida et al. (1995) performed, under the same fracture mode, a comparison between the stress intensity factors obtained by the speckle photography and those obtained by J-integral formulation. Using the elastic-viscoplastic constitutive model, Liang *et al.* (2014) established a mechanical model of the dynamic propagation interface crack for the compression-shear mixed mode.
Specifically regarding methods for calculating the coefficients of asymptotic fields in the vicinity of the crack tip, several analytical and numerical studies have been carried out in recent decades. Most of them are based on the finite element method FEM. Sinclair *et al.* (1984) then developed path independent integrals to calculate stress intensity factors.
Some other authors Kfouri (1986); Toshio and Parks (1992); Ayatollahi *et al.* (1998); Chen *et al.* (2001) worked on computing the elastic T-stress. Using a hybrid crack element, Karihaloo and Xiao (2001) proposed, by means of the p-adaptivity property, an accurate determination of the coefficients of an elastic crack tip asymptotic field, under mixed mode loading. Several other approaches have been introduced for calculating Williams' asymptotic expansion coefficients. These respectively include: (a) the fractal finite element method FFEM Su and Feng (2005); Su and Fok (2007), (b) the over-deterministic method which is based on both FEM and the least squares technique Ayatollahi and Nejati (2011a, 2011b), (c) the symplectic expansion method used to calculate the stress intensity factors for both an edge interface crack and an interface V-notch in a biomaterial plate under bending Zhou et al. (2013). Later, Wang (2017) implemented the symplectic duality system to evaluate the stress intensity factor for interface V-shaped notches in a bi-material Kirchhoff plate bending. More recently, Yao *et al.* (2018) performed a coupling between the asymptotic expansion technique and the finite element method to evaluate V-notches stress intensity factors.

2. Problem Formulation

Let us consider in a polar coordinate system (r,θ), a semi-infinite mixed mode crack in an elastic and isotropic material with crack, characterized by Young's modulus E and Poisson's ratio ν. The system origin O is located at the crack tip. Using the following variables change:

$$\begin{cases} \xi = \ln(r) \\ S_{rr} = r\sigma_{rr} \\ S_{r\theta} = r\sigma_{r\theta} \\ S_{\theta\theta} = r\sigma_{\theta\theta} \end{cases}$$

It then comes out, when neglecting volume forces and assuming the dynamic effects' absence:

Equilibrium Equations

$$\begin{cases} \partial_\xi S_{rr} + \partial_\theta S_{r\theta} - S_{\theta\theta} = 0 \\ \partial_\xi S_{r\theta} + \partial_\theta S_{\theta\theta} + S_{r\theta} = 0 \end{cases} \quad (1)$$

Stress-Displacement Relationships

$$\begin{cases} \partial_\xi u_r = \dfrac{S_{rr} - \nu S_{\theta\theta}}{E} \\ u_r + \partial_\theta u_\theta = \dfrac{S_{\theta\theta} - \nu S_{rr}}{E} \\ \partial_\xi u_\theta - u_\theta + \partial_\theta u_r = \dfrac{2(1+\nu) S_{r\theta}}{E} \end{cases} \quad (2)$$

$\sigma_{rr}, \sigma_{r\theta}, \sigma_{\theta\theta}$ are the stress field components, u_r and u_θ respectively represent the radial and angular displacements fields. Hellinger-Reissner's variational principle can then be written as:

$\delta\Omega = 0$

$$\Omega = \int_{-\pi}^{\pi}\int_{-\infty}^{\infty} (S_{rr}\partial_\xi u_r + S_{\theta\theta}(u_r + \partial_\theta u_\theta) + S_{r\theta}(\partial_\xi u_\theta - u_\theta + \partial_\theta u_r) - \frac{S_{rr}^2 + S_{\theta\theta}^2 - 2\nu S_{rr}S_{\theta\theta} + 2(1+\nu)S_{r\theta}}{2E}) d\xi d\theta \quad (3)$$

3. Mathematical Investigations

Depending on whether the variation in Equation 3 is considered with respect to either S_{rr} or $S_{\theta\theta}$, the following two sub-problems then result:

3.1. $S_{\theta\theta}$ Sub-Problem

Equation 2_1 leads to:

$$S_{rr} = \nu S_{\theta\theta} + E\partial_\xi u_r \quad (4)$$

Combining Equations 3 and 4, it comes out:

$\delta\Omega = 0$, $\Omega =$

$$\int_{-\pi}^{\pi}\int_{-\infty}^{\infty} (S_{r\theta}\partial_\theta u_r + S_{\theta\theta}\partial_\theta u_\theta + S_{\theta\theta}(u_r + \nu\partial_\xi u_r) + S_{r\theta}(\partial_\xi u_\theta - u_\theta) + \frac{(\partial_\xi u_\theta)^2 E}{2} - \frac{(2(1+\nu)S_{r\theta}^2 + (1-\nu^2)S_{\theta\theta}^2}{2E}) d\xi d\theta \quad (5)$$

u_r, u_θ, $S_{r\theta}$ and $S_{\theta\theta}$ being considered as independent variables, the problem to be solved can be written as follows:

Find the unknown vector

$$\tilde{v}(\tilde{q}, \tilde{p}) = \{\tilde{q}^T, \tilde{p}^T\} \quad (6)$$

such that $\dot{\tilde{v}}(\tilde{q},\tilde{p}) = \tilde{H}\tilde{v}(\tilde{q},\tilde{p})$ where $\tilde{q} = (u_r, u_\theta)^T$ and $\tilde{p} = (S_{r\theta}, S_{\theta\theta})^T$ with $\dot{(\,)} = \partial_\theta(\,)$ and

$$\tilde{H} = \begin{pmatrix} \tilde{A} & \tilde{B} \\ \tilde{C} & \tilde{D} \end{pmatrix}, \quad \tilde{A} = \begin{pmatrix} 0 & 1-\partial_\xi \\ -\nu\partial_\xi - 1 & 0 \end{pmatrix}, \quad \tilde{B} = \begin{pmatrix} \frac{2(1+\nu)}{E} & 0 \\ 0 & \frac{1-\nu^2}{E} \end{pmatrix}, \quad \tilde{C} = \begin{pmatrix} -E\partial_\xi^2 & 0 \\ 0 & 0 \end{pmatrix},$$

$$\tilde{D} = \begin{pmatrix} 0 & 1-\nu\partial_\varsigma \\ -1-\partial_\varsigma & 0 \end{pmatrix}$$

3.2. S_{rr} Sub-Problem

Equation 2_2 provides:

$$S_{\theta\theta} = \nu S_{rr} + E(u_r + \partial_\theta u_\theta) \tag{7}$$

Combining Equations 3 and 7, Hellinger-Reissner's variational problem involves:

$$\delta\Omega = 0, \ \Omega = \int_{-\pi}^{\pi}\int_{-\infty}^{\infty} (S_{rr}\partial_\xi u_r + S_{r\theta}\partial_\xi u_\theta + S_{rr}(u_r + \partial_\theta u_\theta)\nu + S_{r\theta}(\partial_\theta u_r - u_\theta) + \frac{(u_r + \partial_\theta u_\theta)^2 E}{2} - \frac{2(1+\nu)S_{r\theta}^2 + (1-\nu^2)S_{rr}^2}{2E}) d\xi d\theta \tag{8}$$

As the variables u_r, u_θ, S_{rr} and $S_{r\theta}$ are independent, the corresponding sub-problem can be formulated as follows:

Find the unknown vector

$$v(q,p) = \{q^T, p^T\}^T \tag{9}$$

such that $\dot{v}(q,p) = Hv(q,p)$ where $q = (u_r, u_\theta)^T$ and $p = (S_{rr}, S_{r\theta})^T$ with $\dot{(\,)} = \partial_\xi(\,)$ and

$$H = \begin{pmatrix} A & B \\ C & D \end{pmatrix}, \quad A = \begin{pmatrix} -\nu & -\nu\partial_\theta \\ -\partial_\theta & 1 \end{pmatrix}, \quad B = \begin{pmatrix} \frac{1-\nu^2}{E} & 0 \\ 0 & \frac{2(1+\nu)}{E} \end{pmatrix}, \quad C = \begin{pmatrix} E & E\partial_\theta \\ -E\partial_\theta & -\partial_\theta(E\partial_\theta) \end{pmatrix},$$

$$D = \begin{pmatrix} \nu & -\partial_\theta \\ -\nu\partial_\theta & -1 \end{pmatrix}.$$

Moreover, the following free traction conditions are applied to the two previous cases:

$$\tilde{p}|_{\theta=\pi} = \tilde{p}|_{\theta=-\pi} = 0 \text{ or } p|_{\theta=\pi} = p|_{\theta=-\pi} = 0 \tag{10}$$

4. Solution Determination

Let us seek the solution as follows:

$$v(\xi,\theta) = \psi(\theta)\mathrm{Exp}(\mu\xi) \text{ or } \tilde{v}(\xi,\theta) = \tilde{\psi}(\theta)\mathrm{Exp}(\mu\xi) \tag{11}$$

The radial and angular problems mentioned above are then reduced to obtaining eigeinsystems respectively:

$$\{\mu, \psi^T(\theta) = \{u_r(\theta), u_\theta(\theta), S_{rr}(\theta), S_{r\theta}(\theta)\}^T\}, \ \{\mu, \psi^T(\theta) = \{u_r(\theta), u_\theta(\theta), S_{r\theta}(\theta), S_{\theta\theta}(\theta)\}^T\}.$$

4. 1. Solution of the Radial Coordinate Problem

From Equations 9 and 11_1, it appears suitable to write:

$$H\psi(\theta)=\mu\psi(\theta) \tag{12}$$

The problem to be solved consists in finding the eigeinsystems $\{\mu,\psi(\theta)\}$ related to the Hamiltonian operator matrix H. In this case, μ being an eigenvalue, the same is true for $-\mu$. On the other hand, the two eigenvectors $\psi_i(\theta)$ and $\psi_j(\theta)$ respectively associated with eigenvalues μ_i and μ_j verify the following adjoint symplectic orthogonality:

$$\left\langle \psi_i^{\mathrm{T}}(\theta),\boldsymbol{J},\psi_j(\theta)\right\rangle=\int_{-\pi}^{\pi}\psi_i^{\mathrm{T}}(\theta)\boldsymbol{J}\psi_j(\theta)\mathrm{d}\theta=\begin{cases}0 & if\ \ \mu_i+\mu_j\neq 0\\ 1 & if\ \ \mu_i+\mu_j=0\end{cases} \tag{13}$$

with $\boldsymbol{J}=\begin{pmatrix}0 & I_2\\ -I_2 & 0\end{pmatrix}$, I_2 the second order unit matrix and $\langle\ .\ \rangle$ the inner product operator. The following theorem then provides the problem solution:

Asymptotic Expansion Theorem

The matrix H is assumed to admit 2n non-zero eigenvalues that can be ordered as follows:

$(\alpha):\ \mu_i,\ Re(\mu_i)<0\quad$ or $\quad Re(\mu_i)=0\cap Im(\mu_i)<0$

$(\beta):\ \mu_{-i}=-\mu_i\quad (i=1,2,...n)$

Especially in group (α), the eigenvalues are classified according to increasing absolute values. More generally, the 2n corresponding eigenvectors constitute a vector basis for the solution space. Any solution can then be expressed as a linear combination of such vectors, as follows:

$$\begin{cases}\nu(\xi,\theta)=\sum_{i=1}^{n}\left(a_i\,\mathrm{e}^{\mu_i\xi}\,\psi_i(\theta)+b_i\,\mathrm{e}^{-\mu_i\xi}\,\psi_{-i}(\theta)\right)\\ a_i=\dfrac{\int_{-\pi}^{\pi}\mathrm{e}^{-\mu_i\xi}\psi_{-i}^{\mathrm{T}}(\theta)\boldsymbol{J}\,\nu(\xi,\theta)\mathrm{d}\theta}{\int_{-\pi}^{\pi}\psi_{-i}^{\mathrm{T}}(\theta)\boldsymbol{J}\,\psi_i(\theta)\,\mathrm{d}\theta};\ b_i=\dfrac{\int_{-\pi}^{\pi}\mathrm{e}^{\mu_i\xi}\psi_i^{\mathrm{T}}(\theta)\boldsymbol{J}\,\nu(\xi,\theta)\mathrm{d}\theta}{\int_{-\pi}^{\pi}\psi_i^{\mathrm{T}}(\theta)\boldsymbol{J}\,\psi_{-i}(\theta)\,\mathrm{d}\theta}\end{cases} \tag{14}$$

In literature, the solution to the problem to be solved is generally obtained on the basis of the radial coordinate, making it tedious to calculate the eigenvectors. However, by expressing the solution on the basis of the angular coordinate and then introducing the exponential matrix method EMM as proposed in this paper, the eigeinsystems can be systematically obtained with extreme ease.

4.2. Solution of the Radial Coordinates Problem and Exponential Matrix Method Background

The introduced method requires for the solution $\tilde{\nu}(\xi,\theta)$ to Problem 6 to be sought in the form11_2, with:

$$\tilde{\psi}(\theta)=exp\left(\tilde{H}(\mu)(\theta+\pi)\right)\tilde{\psi}(-\pi) \tag{15}$$

Consequently, to determine the parameter μ and the initial vector $\tilde{\psi}(-\pi)$, we first consider $\theta=\pi$. Equation 15 then becomes:

$$\begin{cases}\tilde{\psi}(\pi)=\{\tilde{q}^T(\pi),\tilde{p}^T(\pi)\}^T=M\,\tilde{\psi}(-\pi)\\ M=exp\left(\tilde{H}(\mu)(2\pi)\right)=\begin{pmatrix}M_{11} & M_{12}\\ M_{21} & M_{22}\end{pmatrix}\end{cases} \tag{16}$$

where M_{ij} (i, j = 1, 2) is a 2X2 matrix. Now, taking the boundary conditions 10 into account, Equation 16 involves:

$$M_{21}\tilde{q}(\theta=-\pi)=\mathbf{0} \tag{17}$$

In this Equation, the symbol $\mathbf{0}$ represents the 2D-zero vector. However, obtaining the initial vector $\tilde{\psi}(-\pi)$ requires the following condition to be satisfied.

$$\det\left(M_{21}\right)=0 \tag{18}$$

The interest of this Equation is to admit the μ values as solutions. Thereafter, the expected corresponding eigensolutions $\tilde{\psi}(\theta)$ can be directly obtained from Equation 15.

4.3. Eigenvalues and Eigenfunctions by means of Exponential Matrix Method

The method outlined above then allows getting:

$$M_{21}=\begin{pmatrix} -\mu E\mathrm{Sin}(2\pi\mu)/2 & 0 \\ 0 & -\mu E\mathrm{Sin}(2\pi\mu)/2 \end{pmatrix} \tag{19}$$

Thereafter, solving Equation 18 provides $\mu=-\frac{1}{2}$ as the value related to the singular solution. Particularly under mode *I* loading, this value corresponds to the eigenvector $\psi_1^I(\theta)$ defined as follows:

$$\psi_1^I(\theta)=\begin{Bmatrix}\psi_{1,1}^I(\theta)\\ \psi_{1,2}^I(\theta)\\ \psi_{1,3}^I(\theta)\\ \psi_{1,4}^I(\theta)\end{Bmatrix}=\frac{3G}{2\sqrt{2\pi}(\chi+1)}\begin{Bmatrix}\frac{1}{G}[\cos\frac{\theta}{2}-\frac{2\chi+1}{3}\cos\frac{3\theta}{2}]\\ \frac{1}{G}[-\sin\frac{\theta}{2}+\frac{2\chi-1}{3}\sin\frac{3\theta}{2}\\ -\cos\frac{\theta}{2}+\frac{7}{3}\cos\frac{3\theta}{2}\\ \sin\frac{\theta}{2}+\sin\frac{3\theta}{2}\end{Bmatrix},\ \chi=\frac{3-\nu}{1+\nu} \tag{20}$$

where G is the shear modulus. Referring to the asymptotic expansion 14, there is clear evidence that the multiplier coefficient related to this eigenvector corresponds to the stress intensity factor K_I, with:

$$K_I=\int_{-\pi}^{\pi} f(\xi,\theta)d\theta=e^{-\frac{\xi}{2}}\int_{-\pi}^{\pi}(r\psi_{1,1}^I(\theta)\sigma_{rr}+r\psi_{1,2}^I(\theta)\sigma_{r\theta}-\psi_{1,3}^I(\theta)u_r-\psi_{1,4}^I(\theta)u_\theta)d\theta \tag{21}$$

On the other hand, the eigenvalue $\mu=-1$ corresponding to the T-stress T, is associated to the eigenvector $\psi_2^I(\theta)$ defined as follows:

$$\psi_2^I(\theta)=\begin{Bmatrix}\psi_{2,1}^I(\theta)\\ \psi_{2,2}^I(\theta)\\ \psi_{2,3}^I(\theta)\\ \psi_{2,4}^I(\theta)\end{Bmatrix}=-\frac{2G}{(\chi+1)\pi}\begin{Bmatrix}-\frac{1}{4G}(\chi+1)\cos 2\theta\\ \frac{1}{4G}(\chi-1)\sin 2\theta\\ 2\cos 2\theta\\ \sin 2\theta\end{Bmatrix} \tag{22}$$

Therefore, the multiplier coefficient related to this eigenvector is equal to half of T-stress, so that it can be obtained:

$$T=2\int_{-\pi}^{\pi} g(\xi,\theta)d\theta=2e^{-\xi}\int_{-\pi}^{\pi}(r\psi_{2,1}^I(\theta)\sigma_{rr}+r\psi_{2,2}^I(\theta)\sigma_{r\theta}-\psi_{2,3}^I(\theta)u_r-\psi_{2,4}^I(\theta)u_\theta)d\theta \tag{23}$$

In the same way, taking the mode *II* loading into account, it is then obtained for $\mu = -\frac{1}{2}$, a corresponding eigenvector $\psi_1^{II}(\theta)$ defined as:

$$\psi_1^{II}(\theta) = \begin{Bmatrix} \psi_{1,1}^{II}(\theta) \\ \psi_{1,2}^{II}(\theta) \\ \psi_{1,3}^{II}(\theta) \\ \psi_{1,4}^{II}(\theta) \end{Bmatrix} = \frac{G}{2\sqrt{2\pi}(\chi+1)} \begin{Bmatrix} \frac{1}{G}[-\sin\frac{\theta}{2} + (2\chi+1)\sin\frac{3\theta}{2}] \\ \frac{1}{G}[-\cos\frac{\theta}{2} + (2\chi-1)\sin\frac{3\theta}{2}] \\ -\sin\frac{\theta}{2} + 7\sin\frac{3\theta}{2} \\ \cos\frac{\theta}{2} + 3\cos\frac{3\theta}{2} \end{Bmatrix} \tag{24}$$

In this case, the multiplier coefficient related to this eigenvector corresponds to the stress intensity factor K_{II} defined as follows:

$$K_{II} = \int_{-\pi}^{\pi} h(\xi,\theta)d\theta = e^{-\frac{\xi}{2}} \int_{-\pi}^{\pi} (r\psi_{1,1}^{II}(\theta)\sigma_{rr} + r\psi_{1,2}^{II}(\theta)\sigma_{r\theta} - \psi_{1,3}^{II}(\theta)u_r - \psi_{1,4}^{II}(\theta)u_\theta)d\theta \tag{25}$$

5. Numerical Examples

To demonstrate the efficiency and accuracy of the proposed method, the finite element method, performed in Abaqus2016 Software, is used to determine K_I, the T-stress and K_{II}, for four mixed mode example problems, under plane stress condition. The values of the Poisson's ration and the Young's modulus are $\nu = 0.25$ and $E = 210GPa$, respectively.
Five rings around the crack tip are then considered at the following selected locations:
$\frac{r}{a} = \frac{1}{12}, \frac{1}{6}, \frac{1}{3}, \frac{1}{2}$ and $\frac{2}{3}$, see Figure 1.

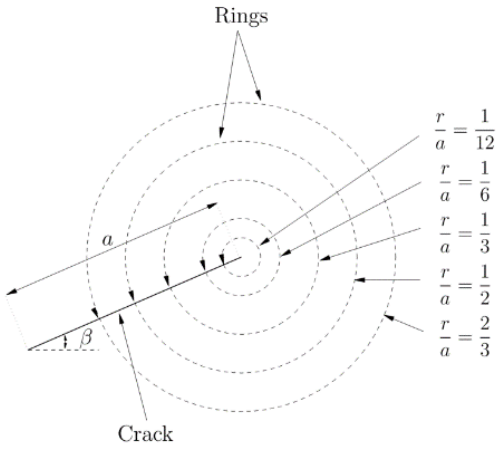

Figure 1. Detail of the crack tip centered rings

A radial mesh is carried out on the domain defined by each ring, with *N* = 181 nodes for a discretization step of two degrees. In order to compare the results obtained by this method with those of literature, several other analyses are performed by increasing the discretization step. Thus, it is obtained for steps of 4, 10, 20 and 40 degrees, a number *N* of nodes equal to 91, 37, 19 and 10, respectively. After each FE analysis, the rings nodal displacements u_r and

u_θ the corresponding nodal stresses σ_{rr} and $\sigma_{r\theta}$ are extracted from the software and used as computer program input data. The trapezoidal integral method TIM implemented in this program, then calculates K_I, the T-stress and K_{II}.

5.1. Example 1. Angled Single Edge Cracked under Uniaxial Tension (ASECT)

The geometrical parameters of the finite plate with an ASECT Figure 2a are $a = 6\,m$, $w = h = 10\,m$, $\beta = 30°$; with the tensile stress $\sigma = 1MPa$.

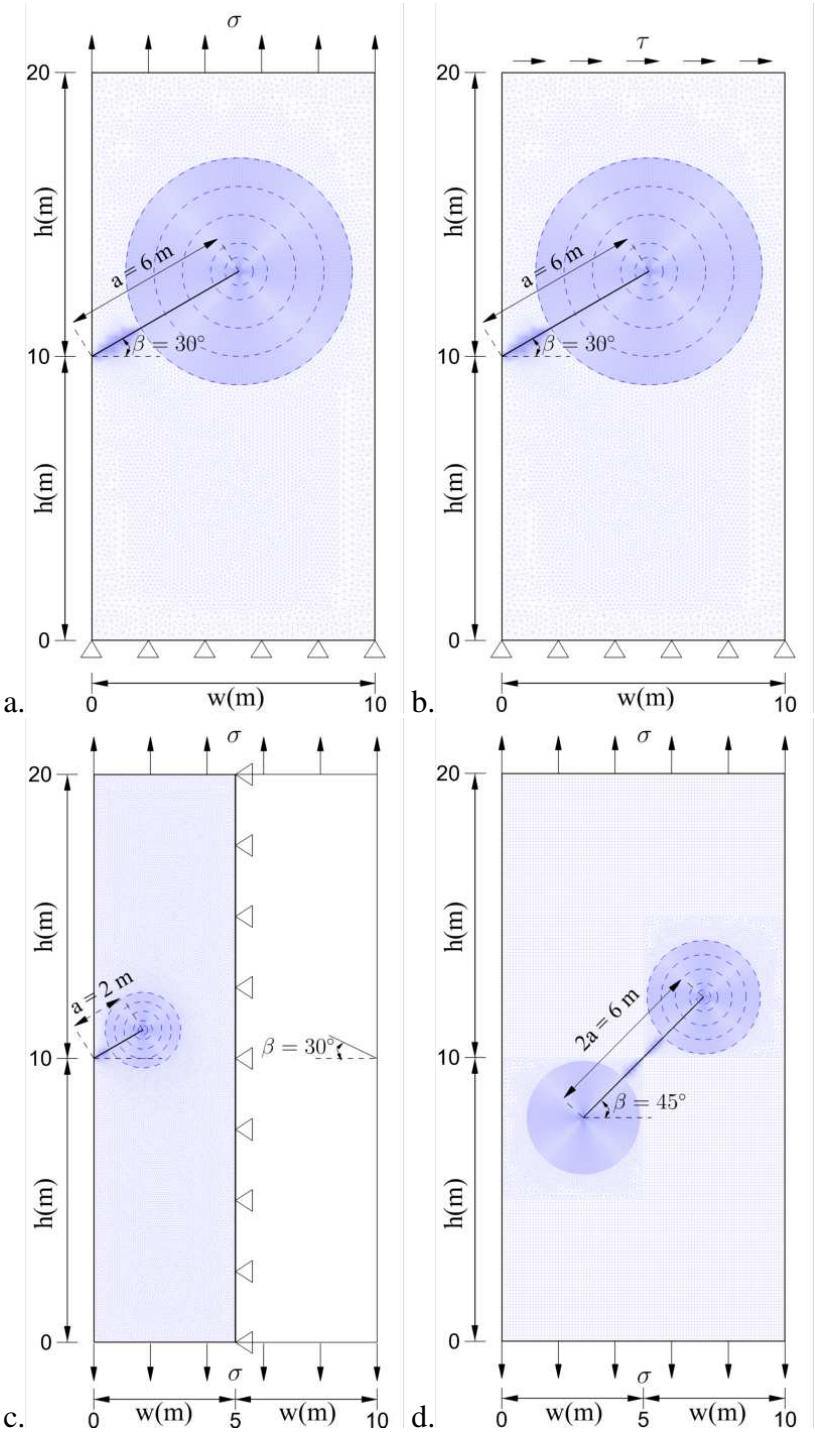

Figure 2. Geometries studied and typical meshes used in the present investigation, a. ASECT, b. ASECS, c. ADECT, d. ACCT

The stress and displacement components calculated by FEM along the five rings are presented in Figures 3a-d.

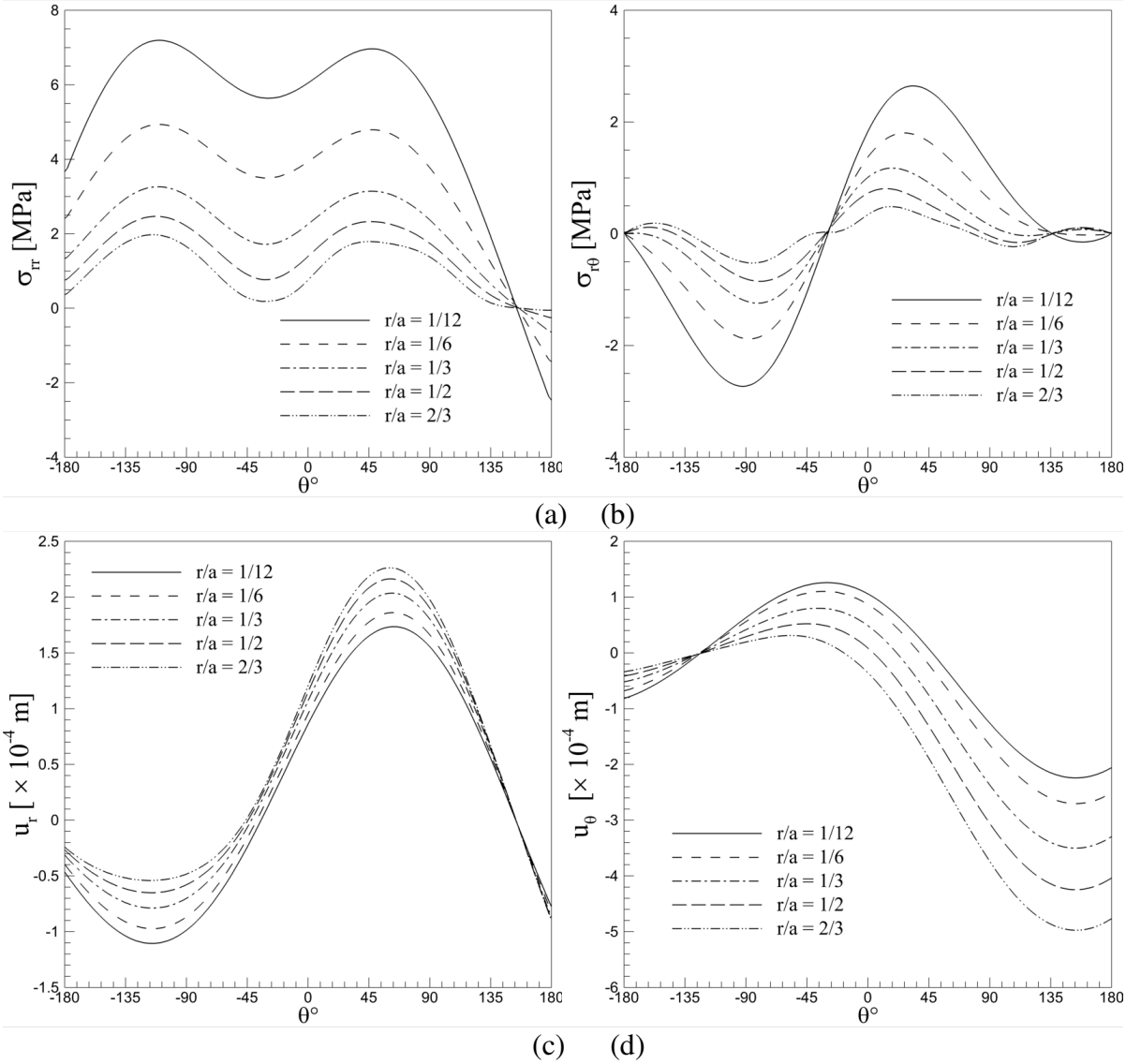

Figure 3. Stress and displacement components along the rings selected around the crack tip for ASECT specimen, a. σ_{rr}, b. $\sigma_{r\theta}$, c. u_r, d. u_θ

Figures 4a-c show the angular distribution of the functions $f(\xi,\theta)$, $g(\xi,\theta)$ and $h(\xi,\theta)$ which result from the stress and displacement components, see Equations 21, 23 and 25 respectively.

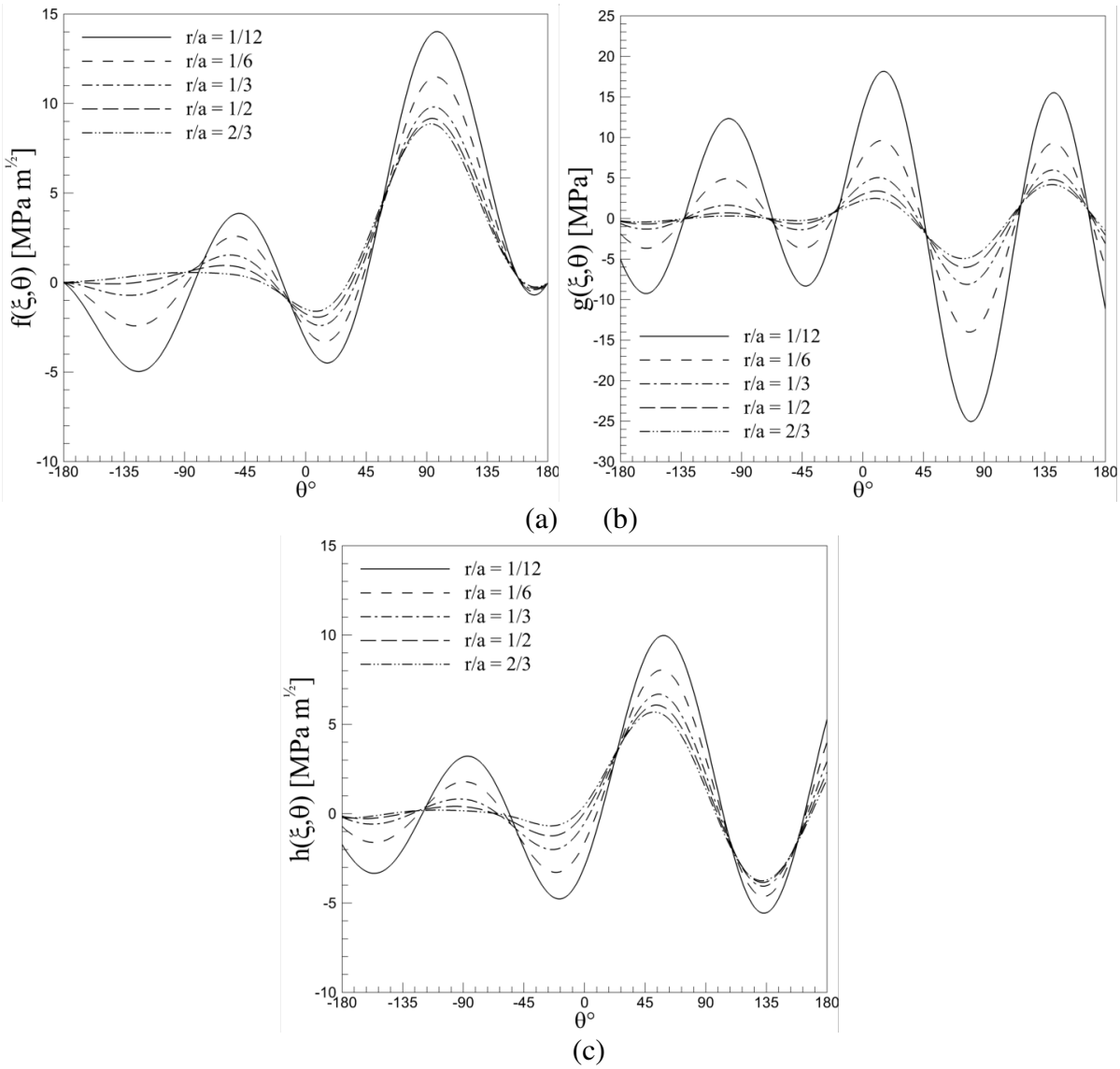

Figure 4. ***Angular distribution of a.*** $f(\xi,\theta)$***, b.*** $g(\xi,\theta)$ ***and c.*** $h(\xi,\theta)$ ***for ASECT specimen***

Using TIM, the numerical integration of these functions provides K_I, the T-stress and K_{II}. To test the accuracy of the proposed method, the values $K_I = 11.048 MPam^{1/2}$, $T = 0.5962 MPa$ and $K_{II} = 2.9981 MPam^{1/2}$ predicted by Abaqus are used as reference solutions. Figures 5a-c represent for increasing values of the number N of nodes, the relative respective errors between the computed values of K_I, the T-stress and K_{II} on the one hand, and the solutions predicted by Abaqus on the other.

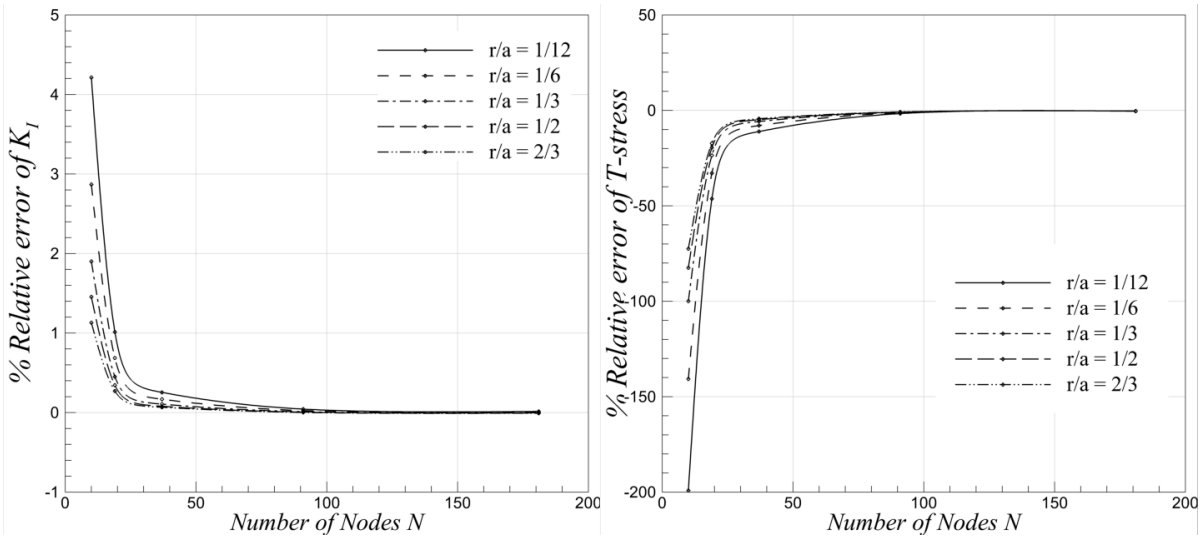

(a) (b)

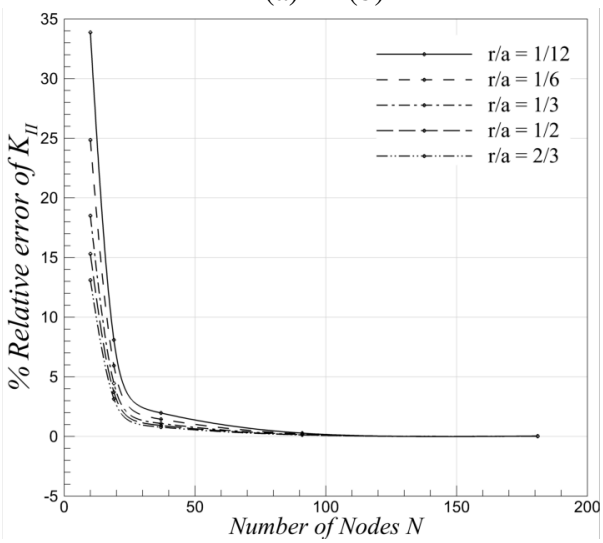

(c)

Figure 5. Percent relative error in a. K_I, b. T-stress and c. K_{II}

As shown by these Figures, K_I, the T-stress and K_{II} steadily converge with a simultaneous increase in the values of N, when N is larger than about 80. The observed relative differences then tend to be acceptable and stable for the five rings. The results computed by the present method with $N = 91$ and $N = 181$ are listed in Table 1, in comparison to literature results.

	$\frac{r}{a}$	Number of Nodes N	$\frac{K_I}{\sigma\sqrt{\pi a}}$	$\frac{T}{\sigma}$	$\frac{K_{II}}{\sigma\sqrt{\pi a}}$
Present study	1/12	91	2.5458	0.5864	0.6925
	1/6	91	2.5453	0.5888	0.6920
	1/3	91	2.5450	0.5904	0.6916
	1/2	91	2.5448	0.5911	0.6915
	2/3	91	2.5447	0.5915	0.6914
	1/12	181	2.5450	0.5938	0.6908
	1/6	181	2.5448	0.5941	0.6908
	1/3	181	2.5446	0.5943	0.6907
	1/2	181	2.5445	0.5944	0.6907
	2/3	181	2.5444	0.5944	0.6907
Abaqus Solution			2.5447	0.5962	0.6905

Ayatollahi and Nejati (2011a, 2011b) FEOD	2.5451	0.5976	0.6910
Xiao et al. (2004) HCE	2.5318	0.5852	0.6868
Xiao et al. (2004) BCM	2.5411	0.5940	0.6896

Table 1. ***K_I, T-stress and K_{II} for ASECT specimen compared with published results*** $\frac{h}{w}=1, \frac{a}{w}=0.6$ ***and*** $\beta=30°$

For the five considered rings, the values of K_I, the T-stress and K_{II} computed by the present method are in very good agreement with those respectively provided by Abaqus software, FEOD method Ayatollahi and Nejati (2011a, 2011b), and HCE and BC methods Xiao *et al.* (2004), respectively.

5.2. Example 2. Angled single edge cracked plate under end shearing ASECS

The geometrical parameters of the finite plate with an ASECS Figure 2b are the same as in Example 1 (ASECT specimen), with the shear stress $\tau=1MPa$. The stress and displacement components along the five rings are presented in Figures 6a-d.

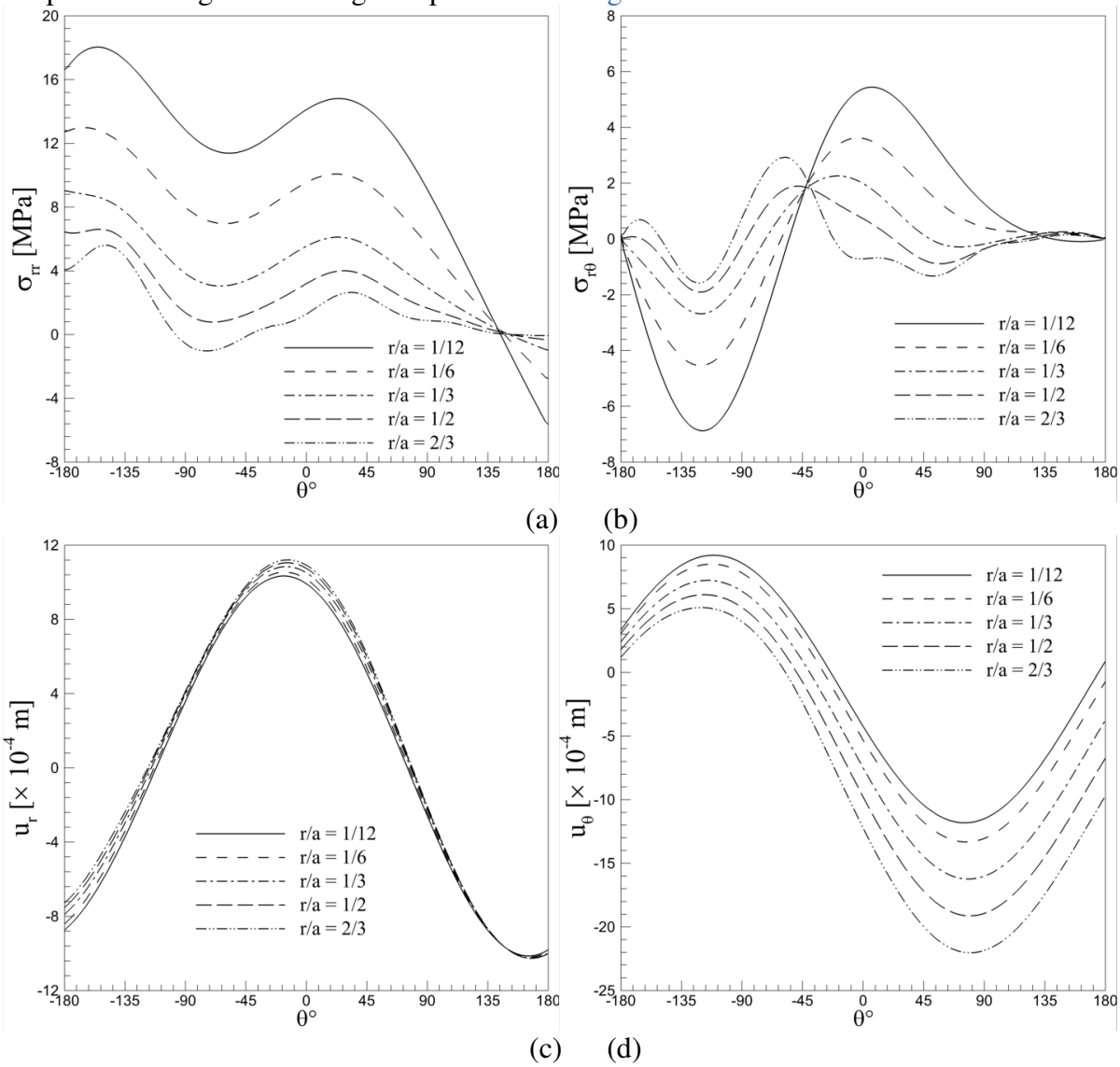

Figure 6. Stress and displacement components along the rings selected around the crack tip for ASECS specimen a. σ_{rr}, b. $\sigma_{r\theta}$, c. u_r, d. u_θ

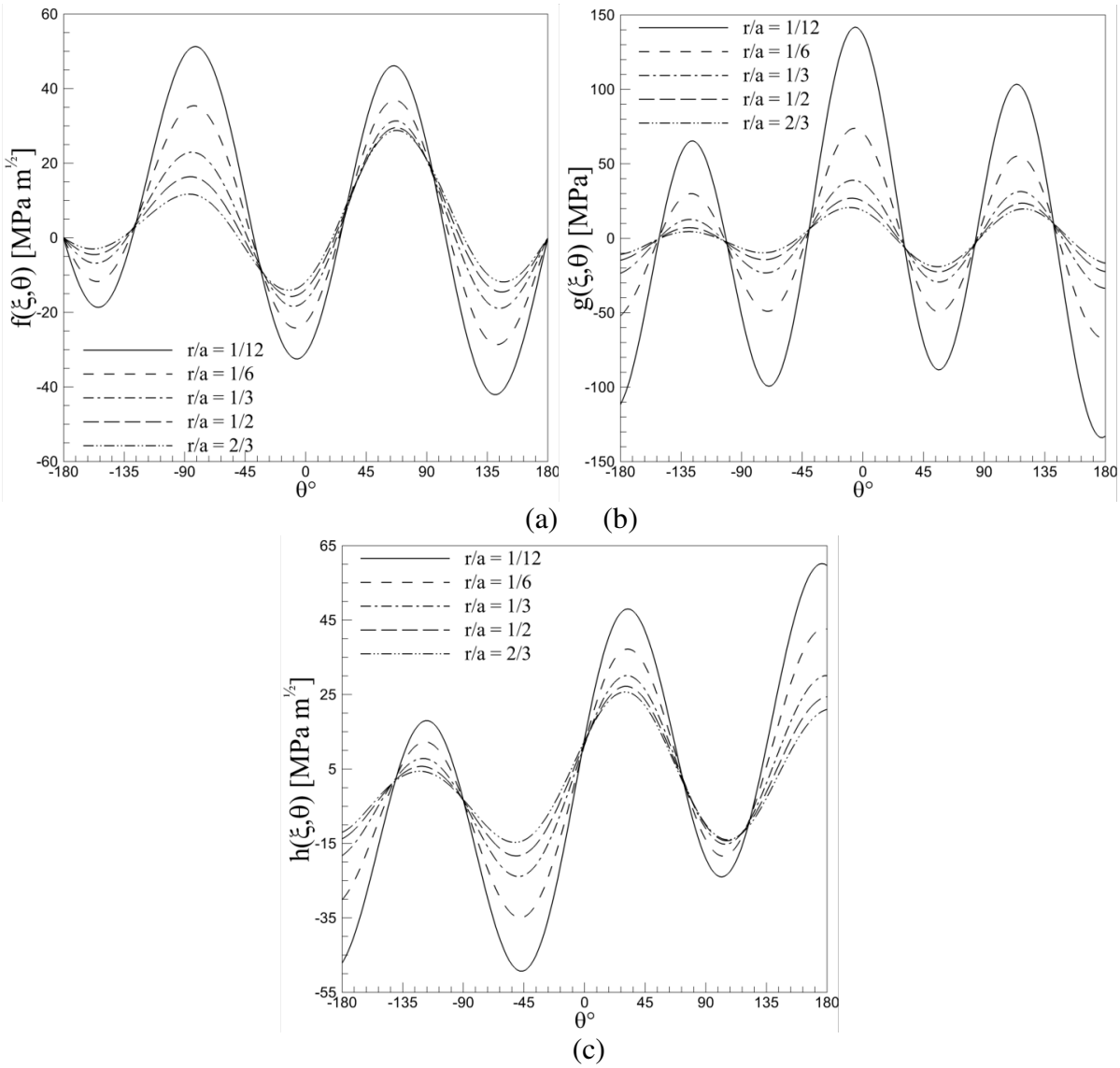

Figure 7. Angular distribution of a. $f(\xi,\theta)$, b. $g(\xi,\theta)$ and c. $h(\xi,\theta)$ for ASECS specimen

The angular distribution of the functions $f(\xi,\theta)$, $g(\xi,\theta)$ and $h(\xi,\theta)$ are presented in Figures 7a-c. The values $K_I = 20.485 MPam^{1/2}$, $T = 5.7802 MPa$ and $K_{II} = 9.8188 MPam^{1/2}$ predicted by Abaqus are used as reference solutions. As in Example 1 (ASECT specimen), the differences observed with respect to K_I, the T-stress and K_{II} tend to become acceptable and stable for values of N larger than 80, as shown in Figures 8a-c.

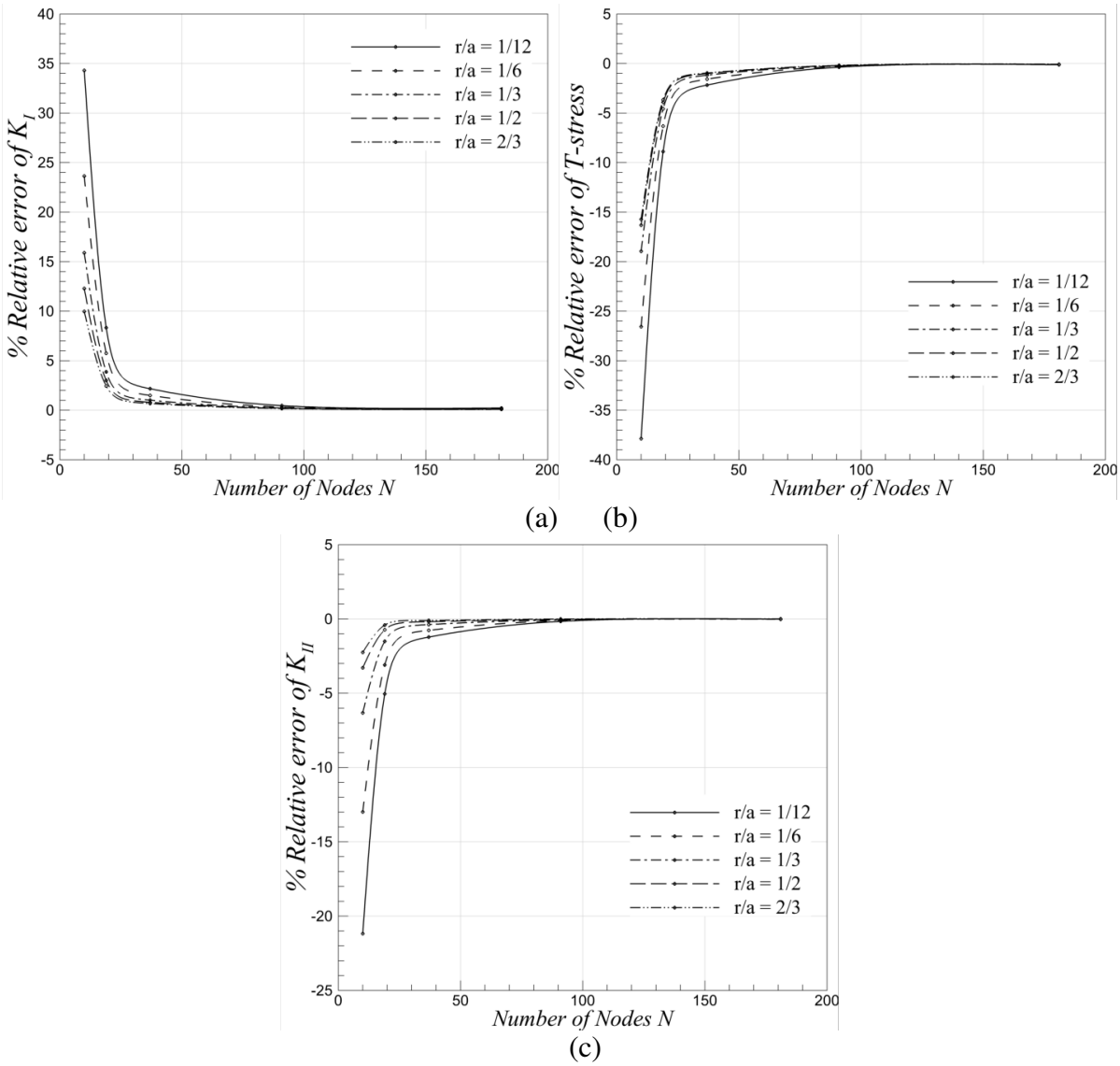

Figure 8. Percent relative error in a. K_I, b. T-stress and c. K_{II}

The results computed by the present method with $N = 91$ and 181 nodes are compared to the literature results in Table 2.

	$\frac{r}{a}$	Number of Nodes N	$\frac{K_I}{\tau\sqrt{\pi a}}$	$\frac{T}{\tau}$	$\frac{K_{II}}{\tau\sqrt{\pi a}}$
Present study	1/12	91	4.7404	5.7592	2.2579
	1/6	91	4.7334	5.7635	2.2590
	1/3	91	4.7290	5.7668	2.2601
	1/2	91	4.7272	5.7685	2.2609
	2/3	91	4.7262	5.7695	2.2614
	1/12	181	4.7290	5.7730	2.2613
	1/6	181	4.7255	5.7737	2.2611
	1/3	181	4.7236	5.7745	2.2612
	1/2	181	4.7229	5.7752	2.2614
	2/3	181	4.7225	5.7758	2.2617
Abaqus Solution			4.7183	5.7802	2.2615
Xiao et al. (2004) HCE			4.6883	5.7376	2.2400
Xiao et al. (2004) BCM			4.1970	5.1776	2.0184

Table 2. ***K_I, T-stress and K_{II} for ASECS specimen compared with published results*** $\frac{h}{w}=1, \frac{a}{w}=0.6$ ***and*** $\beta=30°$

Table 2 shows that the values of K_I, the T-stress and K_{II} computed by the present method for the five considered rings are in very good agreement with those predicted by Abaqus, and those calculated by means of HCE method Xiao *et al.* (2004). The accuracy obtained is better than that of BC method Xiao *et al.* (2004).

5.3. Example 3. Angled double edge cracked plate under uniaxial tension ADECT

The geometrical parameters of the finite plate with an ADECT Figure 2c are $a=2m, w=5m, h=10m, \beta=30°$; with the tensile stress $\sigma=1MPa$. Due to the symmetry in geometry and loading conditions, only one half of the ADECT *i.e.* the left part in Figure 2c is considered. Figures 9a-d show the stress and displacement components along the five rings, while Figures 10a-c present the angular distribution of the functions $f(\xi,\theta)$, $g(\xi,\theta)$ and $h(\xi,\theta)$.

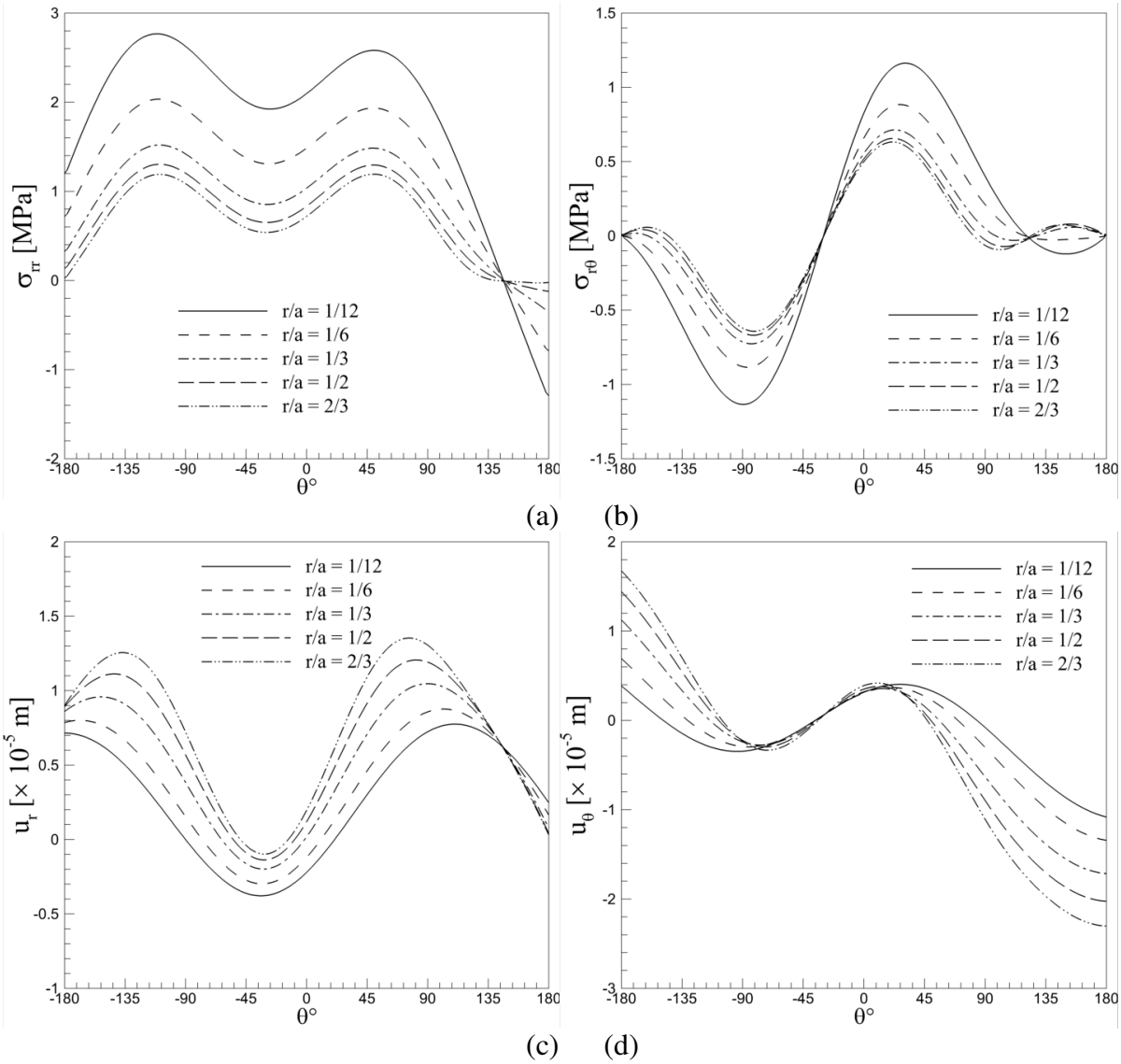

***Figure 9**. Stress and displacement components along the rings selected around the crack tip for ADECT specimen a.* σ_{rr}, *b.* $\sigma_{r\theta}$, *c.* u_r, *d.* u_θ

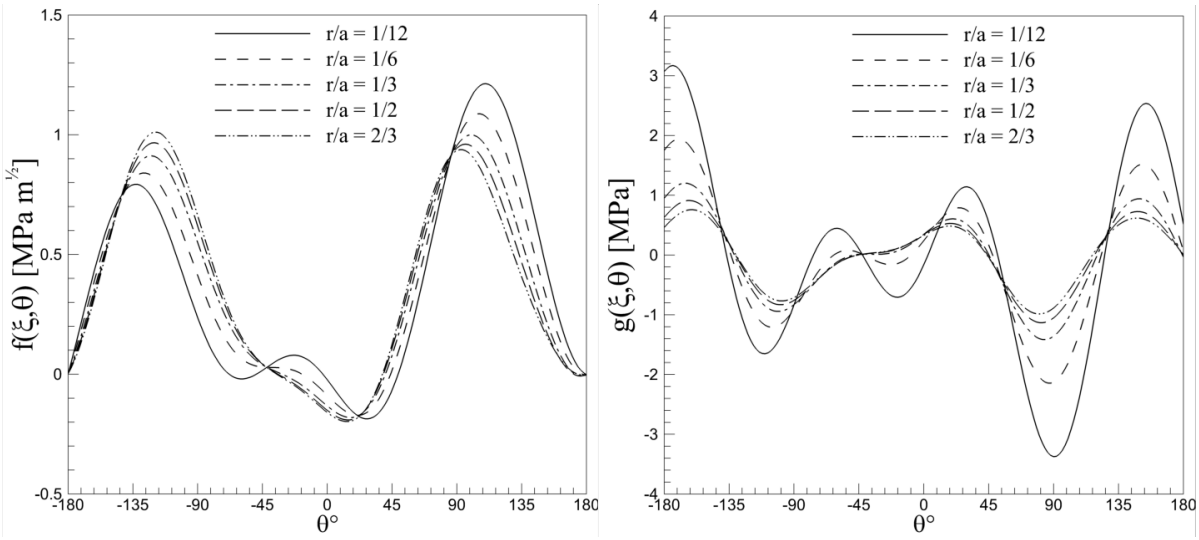

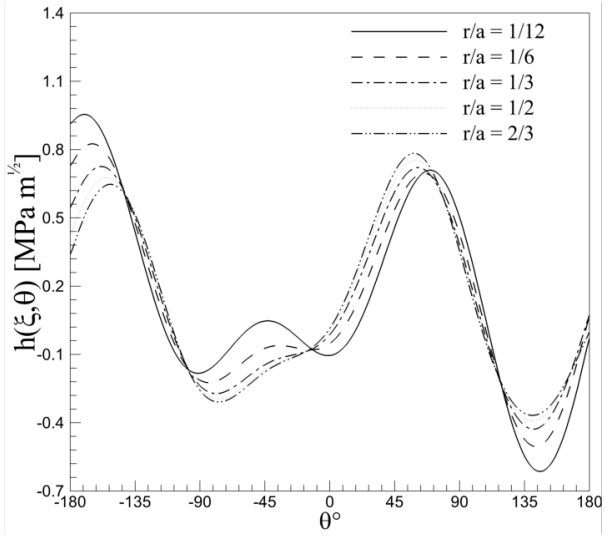

***Figure 10**. Angular distribution of a.* $f(\xi,\theta)$, *b.* $g(\xi,\theta)$ *and c.* $h(\xi,\theta)$ *for ADECT specimen*

The following values predicted by Abaqus are used as reference solutions**:** $K_I = 2.3078 MPam^{1/2}$, $T = -0.1097 MPa$ and $K_{II} = 0.7686 MPam^{1/2}$.

As in Examples 1 and 2, Figures 11a-c show that the differences observed with respect to K_I, the T-stress and K_{II} tend to become acceptable and stable for values of *N* larger than 80.

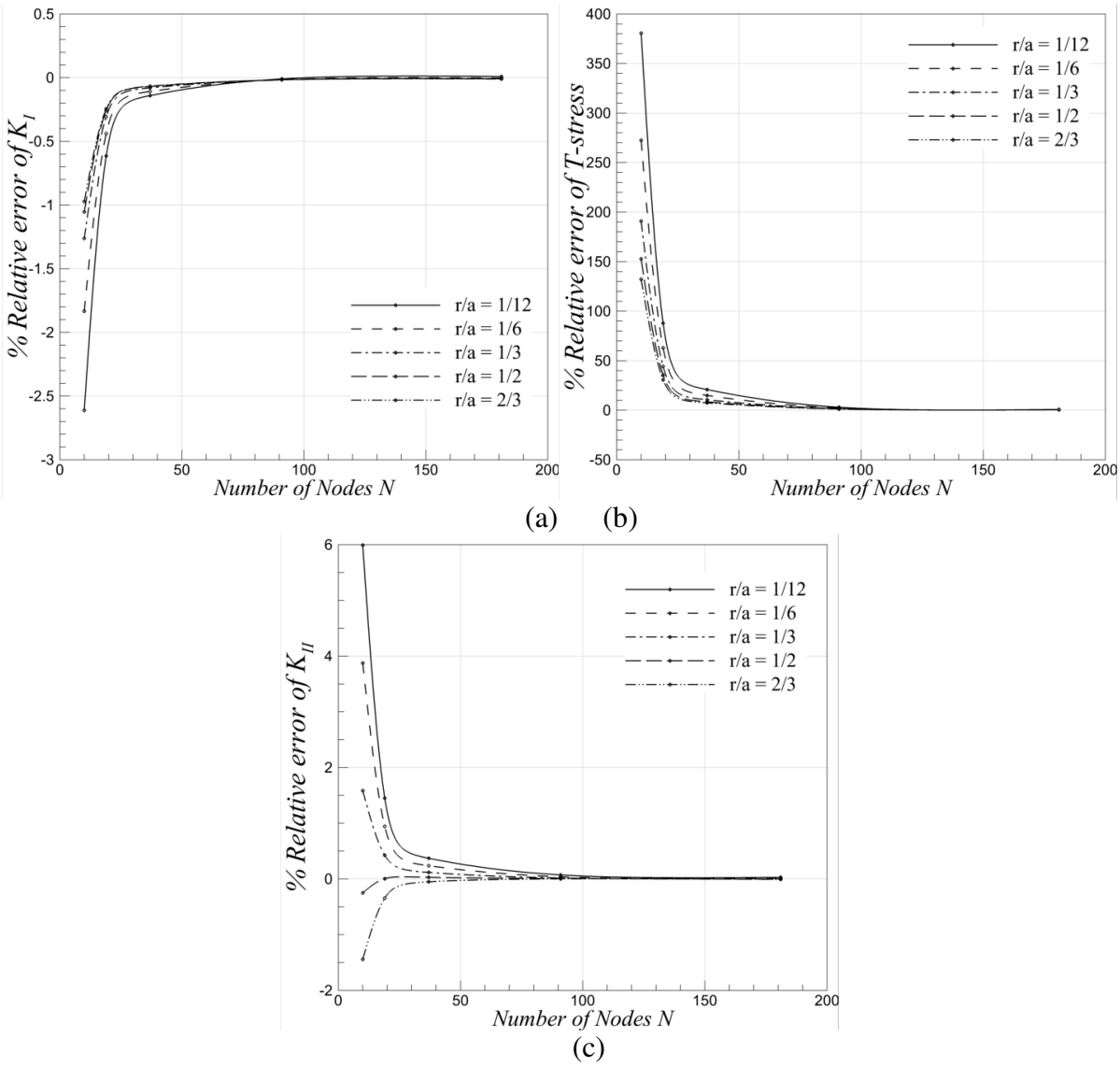

Figure 11. Percent relative error in a. K_I, b. T-stress and c. K_{II}

For the five considered rings, Table 3 shows that the values of K_I, the T-stress and K_{II} computed by the present method; with 91 and 181 nodes, are in very good agreement with those predicted by Abaqus. The accuracy obtained is better than those calculated, using FEOD and BC methods Ayatollahi and Nejati (2011a, 2011b).

	$\frac{r}{a}$	Number of Nodes N	$\frac{K_I}{\sigma\sqrt{\pi a}}$	$\frac{T}{\sigma}$	$\frac{K_{II}}{\sigma\sqrt{\pi a}}$
Present study	1/12	91	0.9206	-0.1131	0.3069
	1/6	91	0.9205	-0.1122	0.3068
	1/3	91	0.9205	-0.1115	0.3067
	1/2	91	0.9205	-0.1112	0.3067
	2/3	91	0.9205	-0.1111	0.3066
	1/12	181	0.9208	-0.1106	0.3067
	1/6	181	0.9206	-0.1103	0.3067
	1/3	181	0.9206	-0.1102	0.3066
	1/2	181	0.9206	-0.1102	0.3066
	2/3	181	0.9206	-0.1102	0.3066
Abaqus Solution			0.9207	-0.1097	0.3066
Ayatollahi and Nejati (2011a, 2011b) FEOD			0.9995	-0.112	0.3309

Ayatollahi and Nejati (2011a, 2011b)	BCM	1.0018	-0.100	0.3332

Table 3. ***K_I, T-stress and K_{II} for ADECT specimen compared with published results*** $\frac{h}{w}=2, \frac{a}{w}=0.4$ ***and*** $\beta=30°$

5.4. Example 4. Angled Center Cracked Plate under Uniaxial Tension ACCT

The geometrical parameters of the finite plate with an ACCT Figure 2d are $a=3m$, $w=5m$, $h=10m$, $\beta=45°$; with the tensile stress $\sigma=1MPa$. The stress and displacement components along the five rings are presented in Figures 12a-d, while the angular distribution of the functions $f(\xi,\theta)$, $g(\xi,\theta)$ and $h(\xi,\theta)$ are shown in Figures 13a-c.

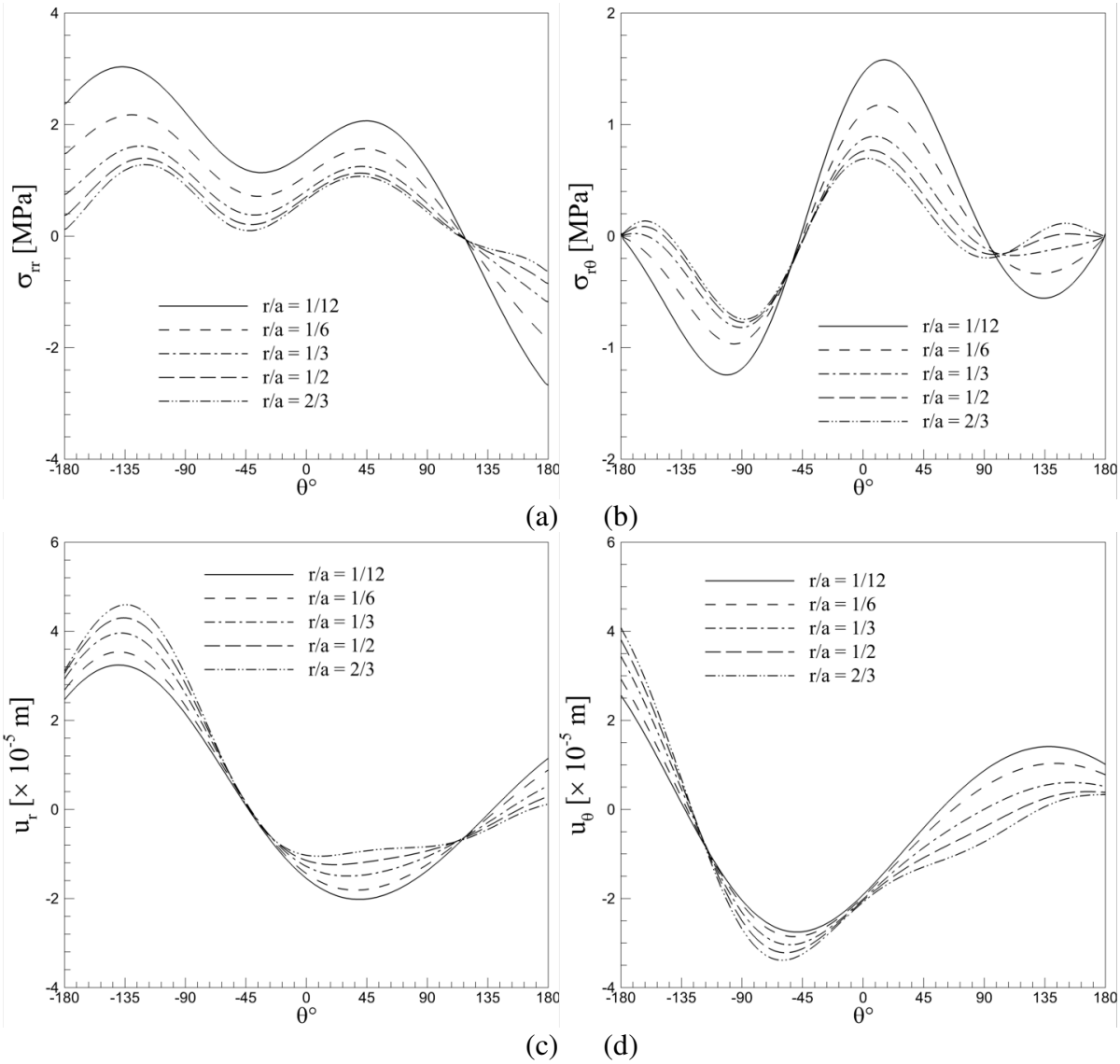

Figure 12. ***Stress and displacement components along the rings selected around the crack tip for ACCT specimen, a.*** σ_{rr}, ***b.*** $\sigma_{r\theta}$, ***c.*** u_r, ***d.*** u_θ

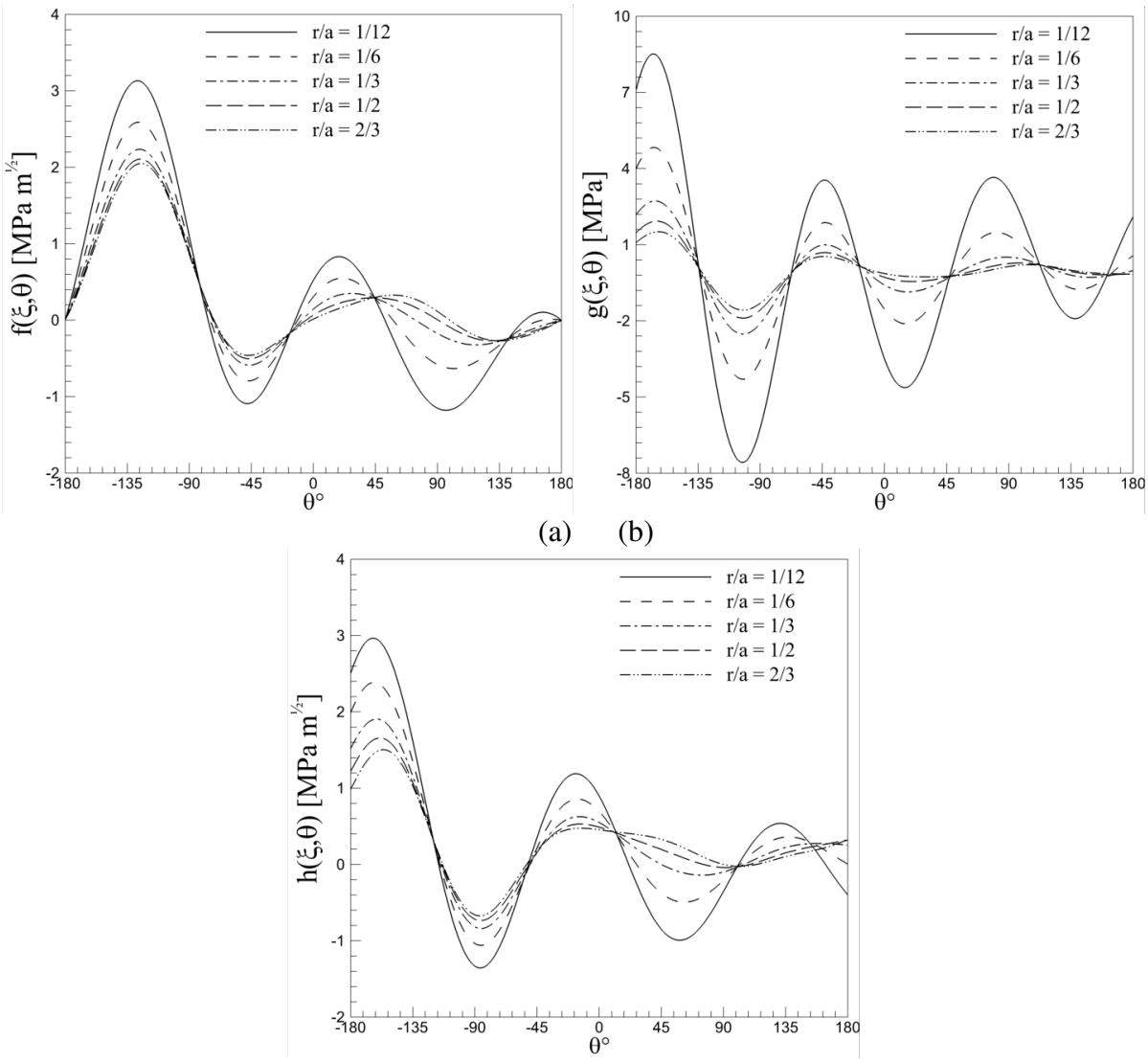

Figure 13. Angular distribution of a. $f(\xi,\theta)$***, b.*** $g(\xi,\theta)$ ***and c.*** $h(\xi,\theta)$ ***for ACCT specimen***

The following values predicted by Abaqus were used as reference solutions: $K_I = 2.0298 MPam^{1/2}$, $T = -0.1561 MPa$ and $K_{II} = 1.7418 MPam^{1/2}$. As in the three previous examples, Figures 14a-c show that the differences observed with respect to K_I, the T-stress and K_{II} tend to become acceptable and stable for values of *N* larger than 80.

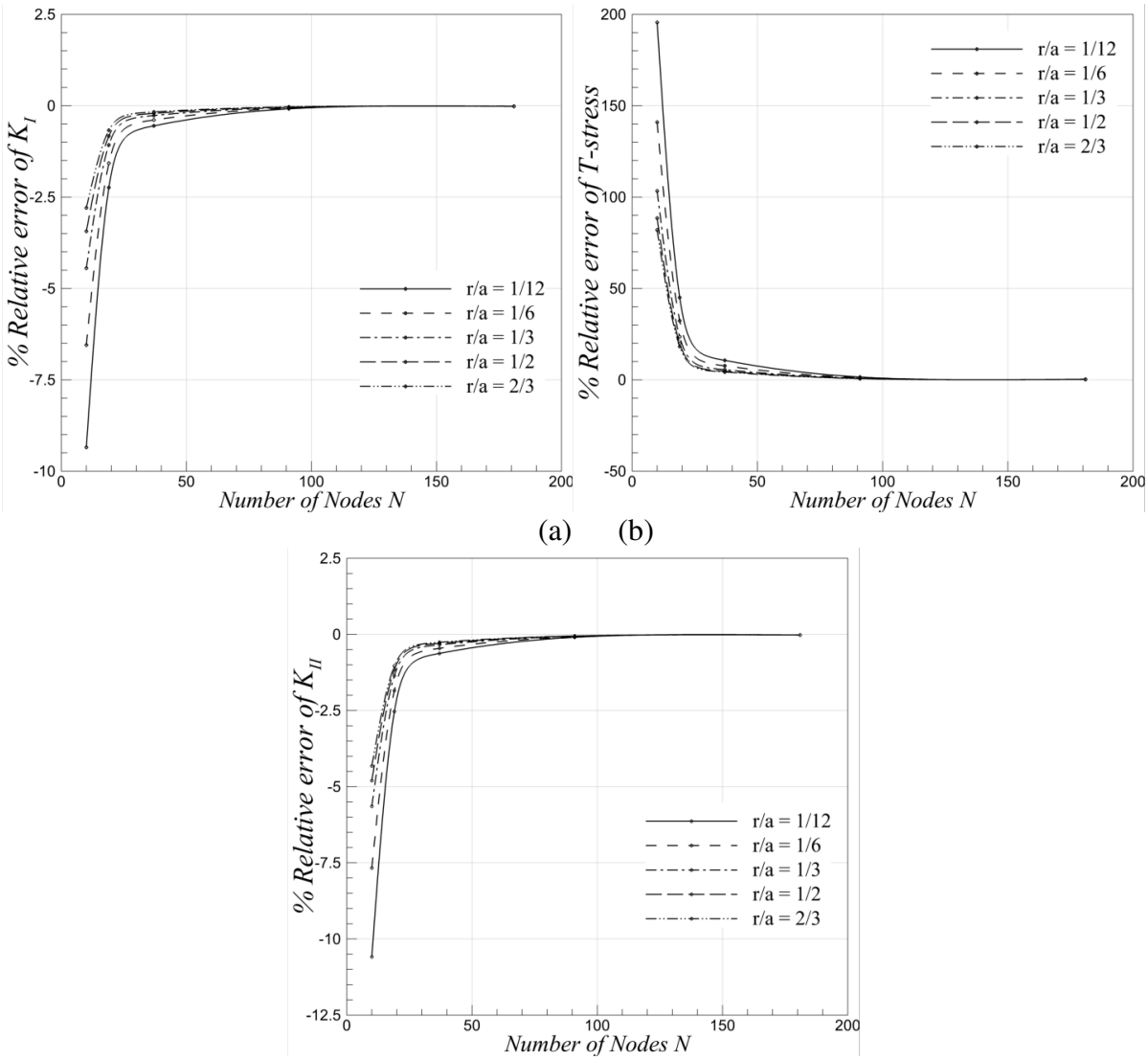

Figure 14. Percent relative error in a. K_I, b. T-stress and c. K_{II}

For the five considered rings, Table 4 shows that the values of K_I, the T-stress and K_{II} computed by the present method, with 91 and 181 nodes, are in very good agreement with those predicted by Abaqus, Kim and Cho (2009) from the RWCI method, and Yang and Ravi Chandar (1999), respectively.

	$\frac{r}{a}$	Number of Nodes N	$\frac{K_I}{\sigma\sqrt{\pi a}}$	$\frac{T}{\sigma}$	$\frac{K_{II}}{\sigma\sqrt{\pi a}}$
Present study	1/12	91	0.6606	-0.1585	0.5668
	1/6	91	0.6607	-0.1579	0.5670
	1/3	91	0.6609	-0.1574	0.5670
	1/2	91	0.6609	-0.1572	0.5671
	2/3	91	0.6610	-0.1571	0.5671
	1/12	181	0.6610	-0.1567	0.5672
	1/6	181	0.6611	-0.1565	0.5672
	1/3	181	0.6610	-0.1565	0.5672
	1/2	181	0.6610	-0.1565	0.5672
	2/3	181	0.6611	-0.1565	0.5672
Abaqus Solution			0.6612	-0.1561	0.5674
Kim and Cho (2009) RWCIM			0.6609	-0.1606	0.5674
Yang and Ravi Chandar (1999)			0.654	-0.1514	0.567

Table 4. ***K_I, T-stress and K_{II} for ACCT specimen compared with published results $\frac{h}{w}=2, \frac{a}{w}=0.6$ and $\beta=45°$***

6. Conclusions

This paper presents the implementation of a new analytical method called exponential matrix method EMM to determine eigensolutions, then to analyze more efficiently, the plane fracture problems of elastic materials in mixed mode I / II Loading. Using this method, the eigenvalues and associated eigenfunctions are obtained more systematically and directly. These satisfy the symplectic orthogonality by formulating the angular stresses from radial ones. The solution to the problem is ultimately in the form of an asymptotic expansion, as in traditional methods. Nevertheless, by means of the present method, the corresponding multiplier coefficients are obtained in a specific and particularly simple process, based on the trapezoidal integration method. The SIFs and T-stress under mixed mode are then calculated. The relevance of the approach implemented in this paper is highlighted by the adequacy of the obtained results with those of literature.

References

Ayatollahi M. R., Pavier M. J. and Smith D. J., 1998, Determination of T stress from finite element analysis for mode I and mixed mode I / II loading, Int. J. Fract., 91(3), 238-298

Ayatollahi M. R. and Nejati M., 2011a, An over deterministic method for calculation of coefficients of crack tip asymptotic field from finite element analysis, Fatigue Fract. Eng. Mater. Struct., 34(3), 159-176

Ayatollahi M. R. and M. Nejati, 2011b, Determination of NSIFs and coefficients of higher order terms for sharp notches using finite element method, Int. J. Mech. Sci., 53(3), 164–177

Chalivendra V. B., 2009, Mixed mode crack tip stress fields for orthotropic functionally graded materials, Acta Mech., 204(1-2), 51-60

Chen C. S., Krause R., Pettit R. G., Banks Sills L. and Ingraffea A. R., 2001, Numerical assessment of T stress computation using a p version finite element method, Int. J. Fract, 107(2), 177-199

Cotterell B., 1966, Notes on the paths and stability of cracks, Int. J. Fract. Mech., 2(3), 526-533

Demir O., Ayhan A. O. and Iriç S., 2017, A new specimen for mixed mode I / II fracture tests : Modeling, experiments and criteria development, Eng. Fract. Mech., 178, 457-476

Dyskin A. V., 1997, Crack growth criteria incorporating non singular stresses: size effect in apparent fracture toughness, Int. J. Fract., 83(2), 191-206

Erdogan F. and Sih G. C., 1963, On the crack extension in plates under plane loading and transverse shear, J. Fluids Eng., 85(4), 519-525

Fett T. and Munz D., 2003, T stress and crack path stability of DCDC specimens, Int. J. Fract., 124(1-2), L165-L170

Gupta M., Alderliesten R. C. and Benedictus R., 2015, A review of T stress and its effects in fracture mechanics, Eng. Fract. Mech., 134, 218-241

Holston Jr A., 1976, A mixed mode crack tip finite element, Int. J. Fatigue, 12(6), 887-899

Karihaloo B. L., 1999, Size effect in shallow and deep notched quasi brittle structures, Int. J. Fract., 95(1-4), 379-390

Karihaloo B. L. and Xiao Q. Z., 2001, Accurate determination of the coefficients of elastic crack tip asymptotic field by a hybrid crack element with p adaptivity, Eng. Fract. Mech, 68(15), 1609-1630

Kfouri A. P., 1986, Some evaluations of the elastic T term using Eshelby's method, Int. J. Fract., 30(4), 301-315

Kim J. K. and Cho S. B., 2009, Effect of second non singular term of mode I near the tip of a V notched crack, Fatigue Fract. Eng. Mater. Struct., 32(4), 346–356

Larsson S. G. and Carlsson A. J., 1973, Influence of non singular stress terms and specimen geometry on small scale yielding at crack tips in elastic plastic materials, J. Mech. Phys. Solids, 21(4), 263-277

Liang W. Y., Wang Z. Q., Liu F. and Liu X. D., 2014, Elastic viscoplastic field at mixed mode interface crack tip under compression and shear, Appl. Math. Mech, 35(7), 887-896

Machida K., Kikuchi M. and Matsushima Y., 1995, Crack tip stress singularity field of a mixed mode three dimensional crack, Mechanical Engineers Series A, 61(581), 1-6

Melin S., 2002, The influence of the T stress on the directional stability of cracks, Int. J. Fract., 114(3), 259-265

Pirmohammad S. and Hojjati Mengharpey M., 2018, A new mixed mode I / II fracture test specimen : Numerical and experimental studies, Theoretical and Applied Fracture Mechanics, 97, 204-214
Ramaswamy S., Tippur H. V. and Xu L., 1993, Mixed mode crack tip deformations studied using a modified flexural specimen and coherent gradient sensing, Experimental Mechanics, 33(3), 218-227
Rice J. R., 1974, Limitations to the small scale yielding approximation for crack tip plasticity, J. Mech. Phys. Solids, 22(1), 17-26
Sinclair G. B, Okajima M. and Griffith J. H., 1984, Path independent integrals for computing stress intensity factors at sharp notches in elastic plates, Int. J. Numer. Meth. Eng., 20(6), 999-1008
Smith D. J., Ayatollahi M. R. and Pavier M. J., 2001, The role of the T stress in brittle fracture for linear elastic materials under mixed mode loading, Fatigue Fract. Eng. Mater. Struct., 24(2), 137-150
Stepanova L. V. and Yakovleva E. M., 2016, Asymptotics of eigenvalues of the nonlinear eigenvalue problem arising from the near mixed mode crack tip stress strain field problems, Numerical Analysis and Applications, 9(2), 159-170
Su R. K. L. and Feng W. J., 2005, Accurate determination of mode I and II leading coefficients of the Williams expansion by finite element analysis, Finite Elem. Anal. Des., 41(11-12), 1175-1186
Su R. K. L. and Fok S. L, 2007, Determination of coefficients of the crack tip asymptotic field by fractal hybrid finite elements, Eng. Fract. Mech, 74(10), 1649-1664
Toshio N. and Parks D. M., 1992, Determination of elastic T stress along three dimensional crack fronts using an interaction integral, Int. J. Solids Struct., 29(13), 1597-1611
Xiao Q. Z., Karihaloo B. L. and Liu X. Y., 2004, Direct determination of SIF and higher order terms of mixed mode cracks by a hybrid crack element, Int. J. Fract., 125(3–4), 207–225
Yao S., Cheng C., Niu Z. and Hu Z., 2018, Evaluation of notch stress intensity factors by the asymptotic expansion technique coupled with the finite element method, Appl. Math. Modeling, 61, 682-692
Yang B. and Ravi Chandar K., 1999, Evaluation of elastic T-stress by the stress difference method, Eng. Fract. Mech., 64(5), 589-605
Wang S., 2017, An analytical singular element for interface V shaped notches in bimaterial Kirchhoff plate bending, Eng. Fract. Mech., 180, 282-295
Williams M. L., 1960, On the stress distribution at the base of a stationary crack, J. Appl. Mech., Transactions ASME, 24(1), 78-82
Zhou Z., Xu X., Leung A. Y. T. and Huang Y., 2013, Stress intensity factors and T stress for an edge interface crack by symplectic expansion, Eng. Fract. Mech., 102, 334-337